

# PROCEEDINGS OF SPIE

[SPIDigitalLibrary.org/conference-proceedings-of-spie](https://spiedigitallibrary.org/conference-proceedings-of-spie)

## Polarization metrology for high numerical aperture DUV objectives

Robert D. Grejda, Paul F. Michaloski, Duncan C. Spaulding, Stephen K. Mack, Robert L. Michaels, et al.

Robert D. Grejda, Paul F. Michaloski, Duncan C. Spaulding, Stephen K. Mack, Robert L. Michaels, Paul G. Dewa, David L. Aronstein, "Polarization metrology for high numerical aperture DUV objectives," Proc. SPIE 11057, Modeling Aspects in Optical Metrology VII, 110570P (21 June 2019); doi: 10.1117/12.2525606

**SPIE.**

Event: SPIE Optical Metrology, 2019, Munich, Germany

# Polarization metrology for high numerical aperture DUV objectives

Robert D. Grejda\*, Paul F. Michaloski, Duncan C. Spaulding, Stephen K. Mack,  
Robert L. Michaels, Paul G. Dewa, David L. Aronstein  
Corning Tropel Corporation, 60 O'Connor Road, Fairport NY 14450

## ABSTRACT

This paper describes an instrument and method for high-resolution characterization of lens components and assemblies for DUV retardance performance at various stages of manufacture. The instrument is a bespoke rotating analyzer Stokes polarimeter designed for DUV wavelengths (e.g. 193 nm, 213 nm, 266 nm, etc.). Using a laser source, the polarimeter delivers a small diameter beam with a characterized polarization state to the optical lens element or objective assembly at the “as-used” design angles of incidence (AOI) to characterize the retardance through the lens or objective at an arbitrary location. The polarization characteristics are usually described by the retardance at specific locations on a component or sub-assembly that can be used to characterize components during development and manufacturing or optimize performance of an assembly.

**Keywords:** polarization, retardance, polarimetry, deep ultra-violet (DUV), birefringence, optical systems

## 1. INTRODUCTION

Lens components and objective assemblies commonly used for DUV lithography or semiconductor inspection systems often have requirements on the polarization performance, including wavefront error and transverse exit-pupil illumination (apodization) as part of the overall imaging or illumination requirements. Generally, the goal is to maintain the polarization state at the object through the imaging objective [1]. Beyond the polarization sensitivity of reflection and refraction at interfaces, some material choices for DUV lens elements will affect polarization performance due to intrinsic birefringence (e.g. crystals), mounting or fabrication stresses, and thin film coatings. Because of non-intrinsic effects, it is preferred to understand the retardance characteristics beyond initial material qualifications. Thus, the goal of this work is to develop metrology as an integral part of the development, fabrication, assembly, and test of the optical sub and final assemblies.

### 1.1 Material retardance characterization

For raw material characterization, stress birefringence is measured by material suppliers in the “blank state” very early in the fabrication process while the material is a plano-plano disk or rectangular solid [2,3]. **Figure 1** shows a typical schematic for a birefringence measurement setup on a material disk. A small diameter beam with a known polarization is transmitted through the disk and changes in polarization are measured with polarization analyzer optics and a detector. The beam position can be rastered across the part to characterize the entire disk and index matching fluid can be used for characterizing material with unpolished surfaces. The measurement is usually reported as the retardance per material thickness, commonly in units of nm/cm. Numerous commercial products are available for this type of evaluation [4,5].

Setups like **Figure 1** are used in for material acceptance testing, where decisions are made to use or discard a particular blank based on the statistics of the birefringence measured. The demanding performance requirements of DUV applications can often only be met when considering the tensor nature of birefringence and characterizing the materials and subsequent lenses along the actual “as-used” design paths in which light will travel through them. For example, for a birefringent material like calcium fluoride (CaF<sub>2</sub>) the light path through the material relative to crystallographic orientation significantly affects the retardance [6]. This situation is further complicated in that finished lenses have nominally spherical or aspherical surfaces, thin film anti-reflection (AR) coatings are present, and lens mounting methods may significantly affect stress birefringence.

\*grejdard@corning.com;

phone 1 585 388-3494;

[www.corning.com/worldwide/en/products/advanced-optics.html](http://www.corning.com/worldwide/en/products/advanced-optics.html)

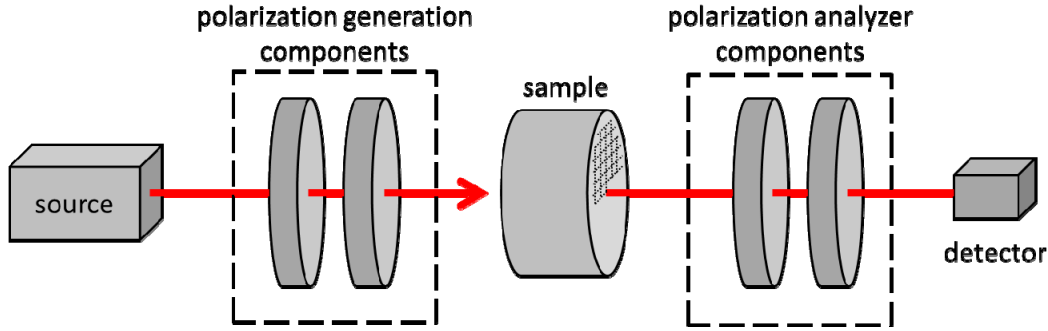


**Figure 1:** The general measurement schematic for material characterization using a source, components for generating a known polarization state and a detector arm with polarization analyzer components (after [4]). The polarized beam or sample can be rastered to evaluate the entire sample.

## 1.2 Stokes polarimetry

Generally, the retardance measurement process shown schematically in **Figure 1** is accomplished through measuring changes in the polarization state of a beam when passing through an optical lens element. The polarization state of a light wave is described here using the electric field amplitudes,  $E_{0x}$  and  $E_{0y}$ , along two orthogonal directions and the phase difference between them,  $\delta$ . These electric field amplitudes are not directly observable quantities, whereas the intensity (time averaged square of the amplitudes) can be measured and used as the basis for establishing “observables of the polarization ellipse” [7]. The mapping of the intensity measurements to electric field amplitudes is done with Stokes parameters shown in series as **Equation 1**, and whose quantities represent the amount of light measured ( $S_0$ ) and the difference in the amounts of orthogonal polarizations states ( $S_1$  through  $S_3$ ).

$$\begin{aligned}
 S_0 &= E_{0x}^2 + E_{0y}^2 & S_0 &= \text{Intensity}_{\text{total}} \\
 S_1 &= E_{0x}^2 - E_{0y}^2 & S_1 &= \text{Linear}_{\text{H-V}} \\
 S_2 &= 2E_{0x}E_{0y} \cos \delta & S_2 &= \text{Linear}_{+45^\circ -45^\circ} \\
 S_3 &= 2E_{0x}E_{0y} \sin \delta & S_3 &= \text{Circular}_{\text{RH-LH}}
 \end{aligned}
 \tag{1}$$

Stokes polarimeters can be made to characterize the polarization state of light; including unpolarized or partially polarized light using the Stokes parameters described above [7]. The simplest version of Stokes polarimeters are generated using combinations of fixed and rotating retarders (wave plates) and polarizers (analyzers) [7,8]. Each version can characterize some or all of the Stokes parameters directly and more complex versions using phase modulators, oscillating elements, gratings, or wavefront division are also possible.

It is important noting that it is often useful to calculate the change of the polarization state along the optical path of a system. For these calculations, the Stokes parameters are vectorized into a 4x1 matrix ( $\mathbf{S}$ ). Stokes vectors can then be used with Mueller matrices ( $\mathbf{M}$ ) to comprehensively describe polarizing properties of a component, using  $\mathbf{S}_{\text{output}} = \mathbf{M} \cdot \mathbf{S}_{\text{input}}$ . While presently our instrument only measures polarization states, it is possible to convert to more complex versions of polarimeters to determine some terms or all 16 terms of the Mueller matrix, providing insight into the nature of polarization state changes caused by the part or sample [7].

For this work, we chose one of the simplest forms of rotating component Stokes polarimeters, the rotating analyzer polarimeter. Because of our interest in making retardance measurements in the DUV, we found this version to be an elegant solution, as polarization components with sufficient quality can be challenging and costly to obtain. The next section will describe more detail of the polarimeter design.

## 2. INSTRUMENT DESIGN

The rotating analyzer polarimeter generalized schematic is shown in **Figure 2**. The source delivers a narrow-diameter beam to two polarization components, a linear polarizer and quarter-wave plate, which are oriented to generate circularly polarized light. This beam is delivered to an area for sample measurements. The beam passes through the sample and then through a linear polarizer (analyzer) which has the ability to rotate around the beam axis. The light is then collected by a detector and recorded.

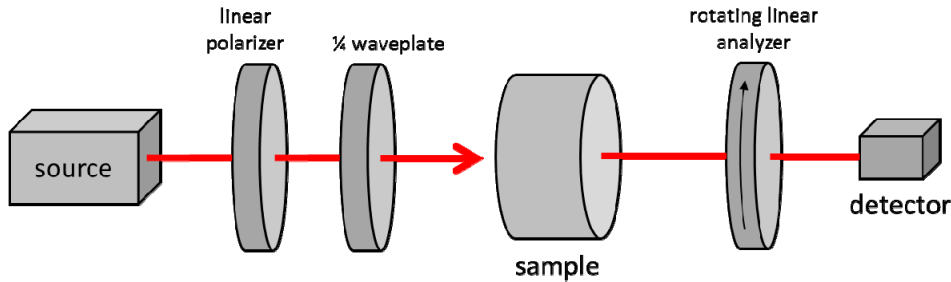


**Figure 2:** Schematic for a generic rotating analyzer Stokes polarimeter.

Because we are interested in measuring optical lenses at the “as-used” design angles of incidence (AOI), we are driven to an instrument design that will either position the beam or sample so that the beam arrives at the correct location and incidence angle on the optical surface. The transmitted beam refracts through the lens or objective assembly and is collected by positioning the detection arm on the analyzer side of the instrument.

### 2.1 Instrument Hardware

Two versions of the instrument described above have been built, as shown in **Figure 3**; one for 266 nm evaluations (**Figure 3a**) and the other for 193 nm (**Figure 3b**) [9]. Fundamentally a single instrument could have been built with the appropriate optics and detectors swapped to accommodate two test wavelengths, but separate instruments were constructed to allow for concurrent testing at each wavelength.

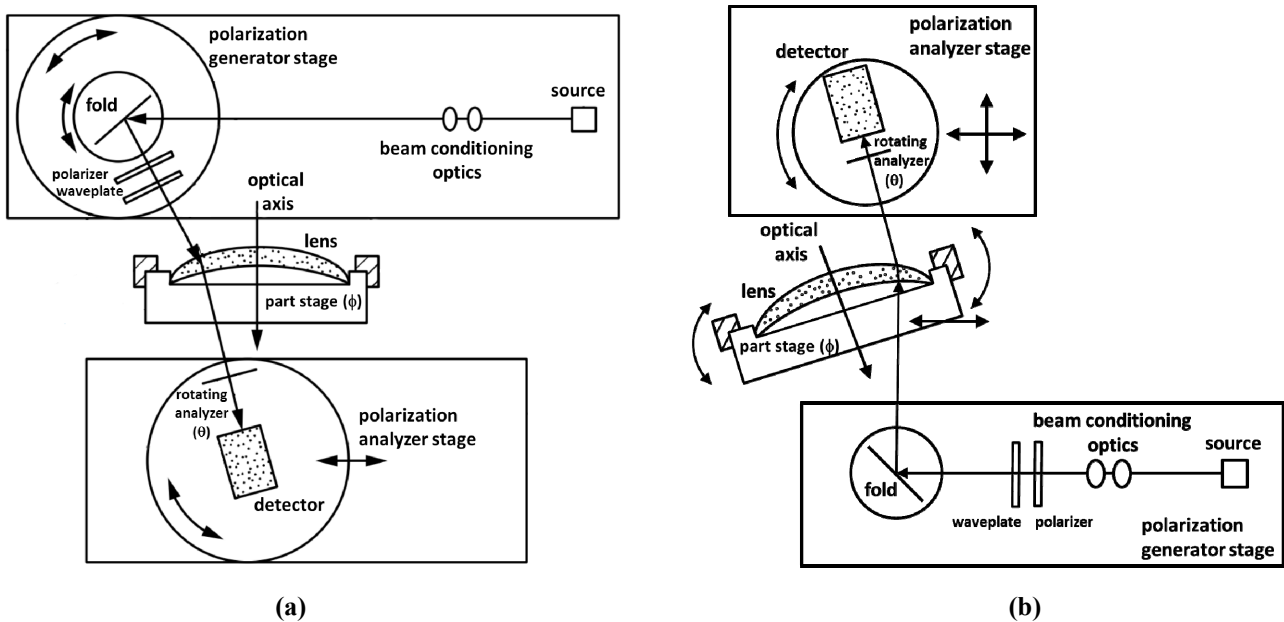


**Figure 3:** (a) Schematic for the 266 nm rotating analyzer polarimeter and (b) for the 193 nm polarimeter.

The beam conditioning optics provide a small (~2mm diameter) beam to the lens under test. Because the lenses tested can have non-zero refractive power, the beam can change size when refracting through the lens so the detector/analyzer is positioned close to the lens to ensure that the entire transmitted beam is recorded at the detector. The analyzer (wire-grid style) is mounted on a rotation stage, providing a rotational degree of freedom,  $\theta$ , about the exiting beam axis just ahead of the detector.

An important feature of both designs is the capability of each part stage to rotate about the optical axis of the lens under test. This rotation axis,  $\varphi$ , allows the retardance performance to be evaluated at a fixed radius circle around the optical axis. It is also important to note that the angle of incidence of the feed beam to the lens under test can be made identical to the as-used incidence angle of light when assembled into an objective. Therefore, the azimuthal retardance data collected can be considered as the component-level contribution to the system retardance in the zone tested and thus used to identify issues, drive design choices, or to compensate and optimize the complete system.

## 2.2 Instrument software

The instrument software has two main components: instrument-operation and data-analysis. The instrument-operation software provides 1) a user interface, 2) control and feedback of the component positioning, 3) control and feedback of the rotating analyzer, and 4) collection of intensity values,  $I$ , from the detector. The intensity data is both a function of part position,  $\varphi$ , and analyzer position,  $\theta$ . Data can be collected with either of these variables being scanned while holding the other one fixed. For the part step/analyzer scan mode, the lens is characterized at a few discrete positions,  $j$ , (i.e.  $\varphi_j$ ) while the analyzer rotates through multiple revolutions (user-defined). Conversely for the part scan/analyzer step mode, the lens can rotate a user-defined number of revolutions while the analyzer is positioned to discrete orientations,  $i$  (i.e.  $\theta_i$ ). Although only a few discrete positions or a fractional rotation of the analyzer are required, multiple revolutions provide uncertainty reduction via averaging. Both modes result in creating a data matrix of intensity values,  $I(\varphi_j, \theta_i)$ .

The analysis software processes multiple data files collected from the instrument operation software. The script performs Fourier-series fitting on the intensity data, plots, and exports results. For a rotating-analyzer polarimeter, the relationship between the intensity,  $I$ , collected as a function of analyzer rotation,  $\theta$ , and the Stokes coefficients are shown in **Equation 2**.

$$I(\varphi_j, \theta_i) = \left[ \frac{a_0}{2} + \frac{a_2}{2} \cos 2\theta + \frac{b_2}{2} \sin 2\theta \right]_{\varphi_j} \quad (2)$$

$$S_0 = a_0$$

$$S_1 = a_2$$

$$S_2 = b_2$$

The coefficients from the Fourier-Series fitting thus identify three of the four Stokes parameters. Note that these intensity series measurements do not directly isolate the  $S_3$  parameter of the polarization. This parameter is calculated using the assumption that depolarization effects are negligible thus the Stokes parameters are related by  $S_0^2 = S_1^2 + S_2^2 + S_3^2$ . The lack of depolarization can be and has been verified via extinction measurements of complete objectives. Thus, the four Stokes parameters characterize the state of polarization of the light. The difference of the state of polarization for the beam passing through the lens under test with the state of polarization determined with the lens removed (also known as an “empty-cavity” measurement) is an estimate of the retardance introduced by the lens.

## 2.3 Referencing and measured retardance (latitude) evaluation

The polarization state of the feed beam is characterized using the stationary part/scanning analyzer mode of the instrument. Review of the resulting Stokes parameters allows the feed polarization to be fine-tuned to minimize ellipticity. The ideal scenario for this measurement setup is to generate a perfectly circular polarization state with the feed beam; this polarization state could be represented by a position at one of the poles of the Poincaré sphere, as shown in **Figure 4** [7]. One salient advantage of using circular polarization is that a priori knowledge of the fast/slow axis

orientation of a retarder (i.e. sample or lens) is not required to estimate the magnitude of the retardance. When the introduction of the part under test causes a movement away from the poles of the Poincaré sphere, the increased ellipticity causes some magnitude of measured retardance that we generically refer to as the “latitude”.

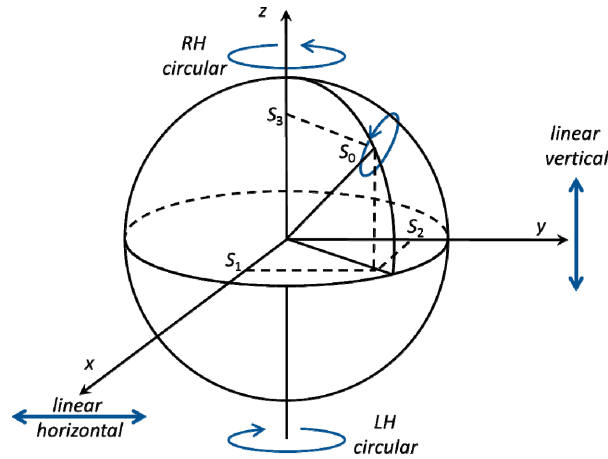


**Figure 4:** Poincaré sphere for depicting the polarization ellipse and its relationship to Stokes parameters after [7].

The latitude term is analogous to the geographic north-south position on a globe and can be calculated from the Stokes parameters using the following relationship shown in **Equation 3**. The latitude value encompasses any effect of the part on the polarization that introduces ellipticity, including bulk material retardance, stress or intrinsic birefringence, or diattenuation at the surfaces. The surface diattenuation is the unequal transmission difference between orthogonal polarization states; which is observed to be a significant impact to latitude for uncoated surfaces at non-normal incidence angles (Fresnel loss), or negligibly small for thin-film anti-reflection coated surfaces.

$$\text{latitude} \approx \delta = \cos^{-1} \left( \frac{S_3}{S_0} \right) \tag{3}$$

Additionally, because of limitations in the performance and adjustment resolution of the polarization generation components, the feed polarization cannot be made perfectly circular. Subsequent measurements of the lens under test are affected by this imperfectly circular (elliptical) polarization of the feed beam. To assess the impact of imperfect circular polarization in this work, we supplement the analysis by creating a model of the measurement using commercially available optical design software, which can simulate the ideal retardance impact of the lens under test with the elliptical feed polarization measured from the empty-cavity reference. The model can also contain material factors like intrinsic birefringence, Fresnel effects from uncoated surfaces, and performance of thin-film coatings. In addition, the modeling results are also invaluable for comparing the measurement results to determine if the retardance behavior of the lens under test is performing within expectation, or if factors related to materials, coating, or mounting are deviating the measured retardance or latitude.

### 3. MEASUREMENT RESULTS

Using a circularly polarized feed beam, most measurements made with the polarimeters described above are azimuthal scans of lenses made at as-used AOIs. Normal data spacing for part scan mode is steps of 0.25° in the azimuthal direction. Noise, measurement reproducibility, and examples of the instrument accuracy and utility for optimization can be assessed using measurements of multiple lenses and objective assemblies, as shown in the following sections.

### 3.1 High purity fused silica at 193 nm

**Figure 5** shows 193 nm retardance measurement results for an uncoated 75 mm diameter by 2.6 cm thick fused silica disk with commercially polished faces purchased to a  $< 1$  nm/cm specification for stress birefringence. The disk is measured at four different AOIs. This measurement set varies both the theoretical diattenuation from the increased AOI of the surfaces and increased the path length through the material due to part tilt. The theoretically calculated diattenuation for a perfectly circular feed polarization is shown for each AOI as the red dashed line in each plot.

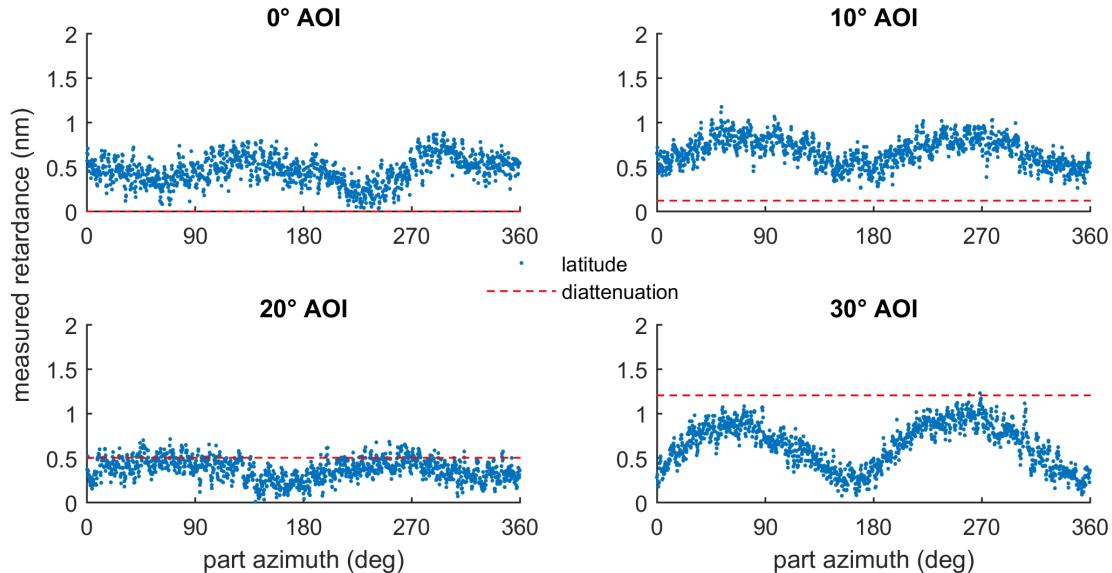


**Figure 5:** Measured azimuthal retardance of an uncoated high purity fused silica disk for 4 different AOIs and the calculated contribution to the measurement from diattenuation for a perfectly circular polarization input.

Initially, it is apparent that although the nominal birefringence is small and below the material specification for a disk of this thickness, the Fresnel effect on the measurement set is not accurately tracked. This is rectified when the modeled performance uses the feed beam polarization that was characterized just prior to the measurement of the sample. **Figure 6** shows that the corrected model matches the measurement average to  $\pm 0.2$  nm exemplifying improved measurement accuracy through referencing with the feed beam polarization. The two-lobed signature in some of the scans locations could be the signature of residual stress birefringence, however, the amplitude is small and well within specification for a disk of this thickness, even when corrected for DUV wavelengths [10].

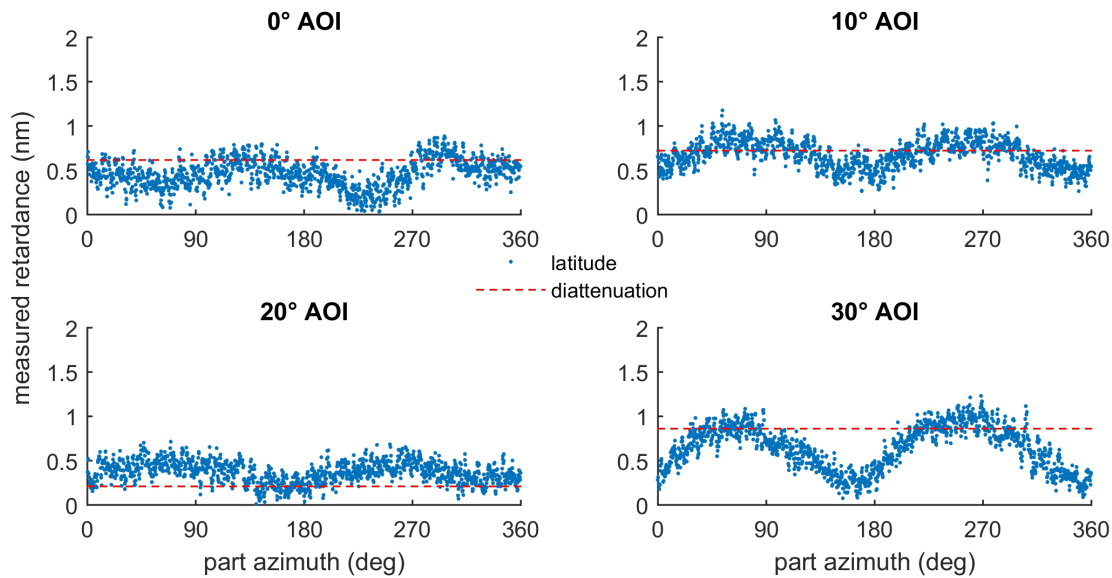


**Figure 6:** Measured azimuthal retardance of an uncoated high purity fused silica disk for 4 different AOIs and the calculated contribution to the measurement from diattenuation when corrected for actual feed beam ellipticity.

### 3.2 Calcium fluoride blanks and lens geometries at 193 nm

Another example of the resolution and reproducibility of the instrument can be seen in the evaluation of measured retardance (latitude) of a calcium fluoride disk measured at 193 nm. The sample disk is commercially polished on the disk faces, is uncoated, and 75 mm diameter by 2.4 cm thick. The faces of the disk are perpendicular to the  $\langle 111 \rangle$  crystal axis to within  $\pm 2^\circ$ . When measured normal to the faces, the intrinsic birefringence is nominally zero for the ideal crystal. As the path through the material deviates from the  $\langle 111 \rangle$  axis the theoretical amount of intrinsic birefringence increases and has  $120^\circ$  symmetry in the azimuthal direction. **Figure 7** shows a schematic of the measurement setup.

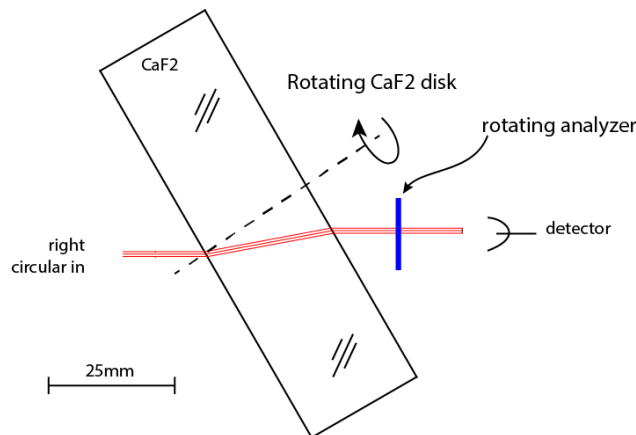


**Figure 7:** Schematic of  $\text{CaF}_2$  disk measurement at 193 nm.

In the schematic, the disk is measured at a  $34^\circ$  AOI, which generates a  $22^\circ$  angle of the ray from the  $\langle 111 \rangle$  axis of the  $\text{CaF}_2$  crystal about which the part rotates during the measurement. This angle in addition to the additional path length through the material generates a significant amount of intrinsic birefringence at 193 nm. Commercial modeling software can show the latitude performance using the ideal material properties of the crystal. The latitude measurement for the disk is shown in **Figure 8** along with the modeled latitude expectation for a perfect crystal.

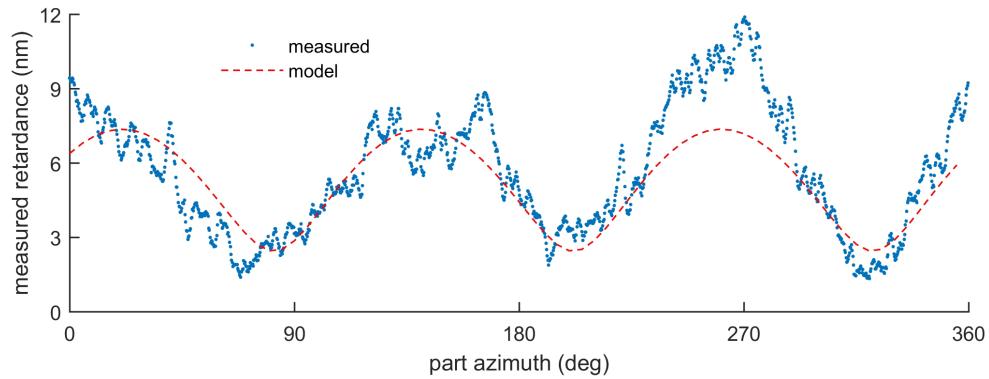


**Figure 8:** Measurement results and modeled prediction for a  $\text{CaF}_2$  disk.

As seen the **Figure 8**, the expected trefoil signature of the  $\text{CaF}_2$  birefringence is seen in the data, however, there is significant amplitude deviations of higher spatial frequency in the measured retardance compared to an ideal crystal. In an effort to understand if these high-frequency features are from the sample or an artifact of the instrument, the sample is measured for a second time but clocked  $90^\circ$  on the part stage. Azimuthal signatures that reside with the sample should rotate with the part if the instrument errors are small and repeatable. **Figure 9** shows the first and second measurements as well as the  $90^\circ$  synthetically rotated back and plotted alongside to the original measurement.

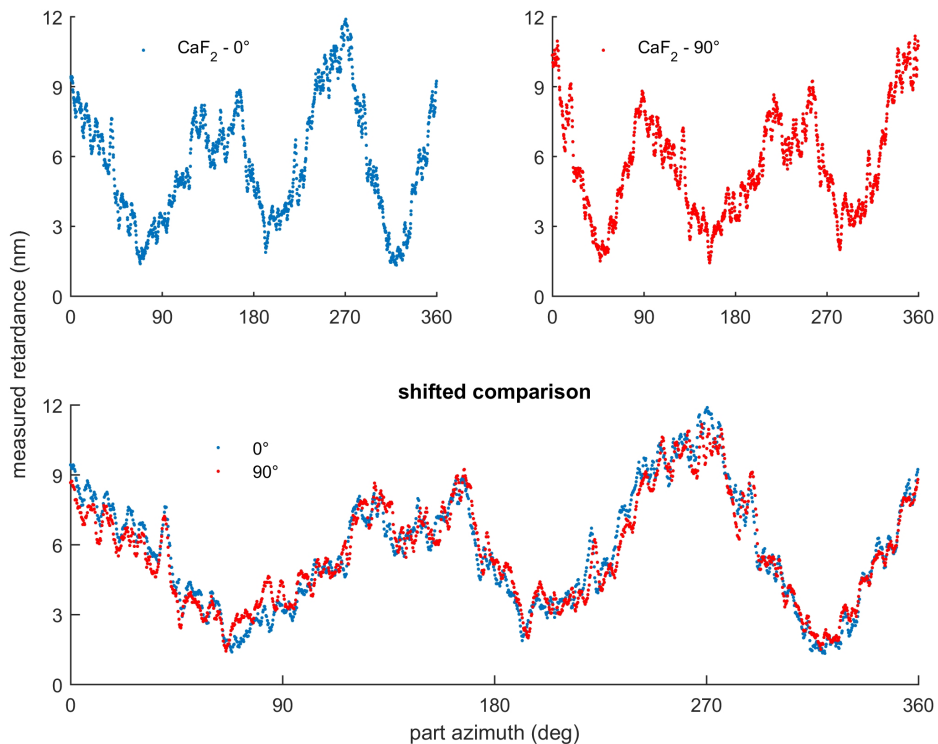


**Figure 9:** Two measurements of a  $\text{CaF}_2$  disk, clocked  $90^\circ$  on the instrument part stage.

Measurements are also made with the 193 nm polarimeter on finished lenses that are fabricated and coated for use in a high numerical aperture (NA) imaging objective. The lenses are produced from both calcium fluoride and high purity fused silica and can be measured at various stages of manufacture, with anti-reflection coatings and mounted in holders. **Figure 10** shows typical results from a 62 mm diameter, meniscus, fused silica lens in a completed state of manufacture and mounted in holders used for assembly. The lens was measured in a zone at 75% of the clear aperture at the as-used

AOI in the final objective assembly. The thickness of material at the zone being tested is 9 mm; the lack of significant latitude in the result indicates the performance of the thin film coatings and the bulk material. The lack of any azimuthal signature indicates low stress mounting of the lens in the holder.

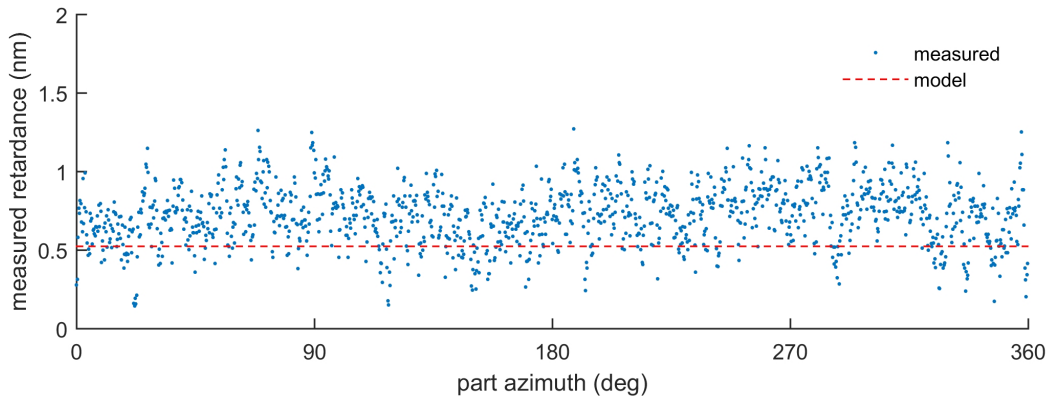


**Figure 10:** Latitude measurement of 193 nm coated lens at the as-used AOI and 75% aperture.

Measurements of calcium fluoride at as-used AOIs and light paths through the crystal can be used to see the effect of intrinsic birefringence on the transmitted light. **Figure 11** shows a typical measured retardance of a 55 mm diameter, meniscus shaped,  $\text{CaF}_2$  lens mounted in holder and complete with thin film coatings. It is also measured at the as-used AOI and in a zone at 75% of the clear aperture. The ray angle with respect to the  $\langle 111 \rangle$  along with the path length through the material of  $\sim 11.5$  mm result in nearly 3 nm P-V of birefringence in this zone.

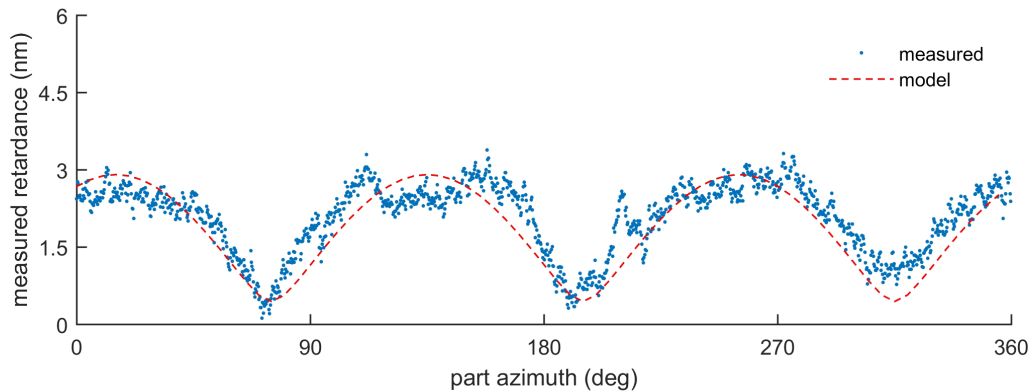


**Figure 11:** Latitude measurement of 193nm  $\text{CaF}_2$  coated lens at as-used AOI and 75% aperture.

### 3.3 Component and system measurements at 266 nm

The 266 nm polarimeter operates fundamentally the same as the 193 nm version and has been frequently used for optimization of optical systems. Azimuthal retardance data from a subset of lenses from an objective measured at the same as-used zone are used to optimize the system by clocking the lenses (i.e. minimize asymmetries via rotation of lenses about their optical axis). **Figure 12** shows the polarimeter results for 5 lenses of an imaging objective. The measurements are made using the part step/analyzer scan mode, collecting retardance data at  $30^\circ$  azimuthal increments on each lens element. Each azimuthal trace represents the polarimeter results of corresponding diameters and AOIs for the most sensitive radial zone of the objective's entrance pupil. The diattenuation is not isolated from the retardance, since it is an insignificant portion of the measurement for the coated surfaces.

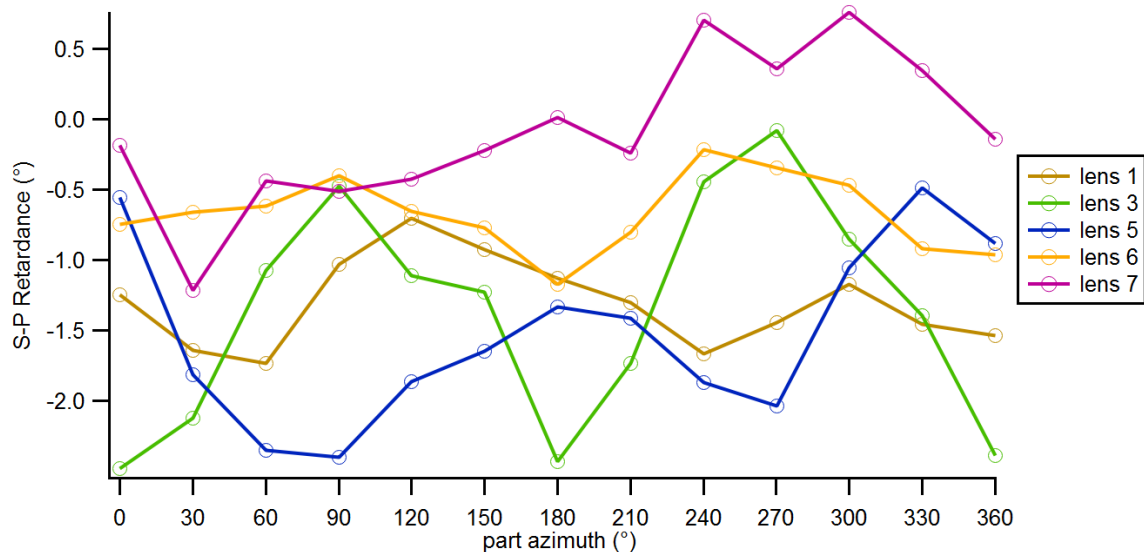


**Figure 12:** Measurement results from 5 lenses on the 266 nm polarimeter.

An example on the polarimeter accuracy and utility is shown in comparing the testing of the complete objective retardance performance to the summation of each lens' contribution. **Figure 13** shows the close correlation between the summation of individual lens elements (abscissa) and the total objective qualification test results (ordinate) for 4 objectives. The qualification of pupil retardance of 0.97 NA imaging objectives is performed via extinction of linear light, which is converted to equivalent retardance. Please note that 3° of retardance is equivalent to only 0.008 waves, or ~2 nm, of phase delay between two orthogonal polarization states, a non-trivial task for a high NA system with high angles of incidence on anti-reflection coated surfaces.

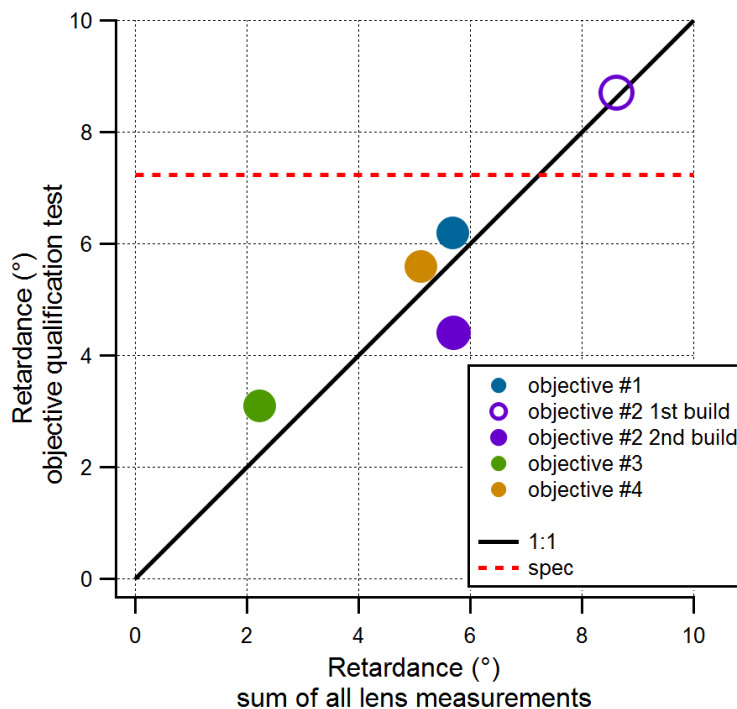


**Figure 13:** A comparison of a complete build of the objective to the summation of the polarimeter measurements of the individual lenses.

The agreement of the data to the 1:1 line provides evidence of the summation method's ability to accurately predict the system level performance and that no significant amount of stress is added in the build of the objective. The utility is illustrated with the two points associated with two different builds of objective #2. Objective #2 was first built with random clocking of the lenses. The 2<sup>nd</sup> build of the objective uses the same lenses however, their clocking is prescribed based on the polarimeter results with the intent on minimizing the total azimuthal retardance variation, thus reducing the objective retardance significantly.

#### 4. CONCLUSIONS

In this work, custom DUV polarimeters were developed to measure retardance characteristics of lens elements in various stages of manufacture and specifically at as-used angles of incidence when incorporated in the objective assembly. The instruments built are Stokes polarimeters which provide retardance information with high resolution for a range of lens geometries and materials. The data from the polarimeters provide information on a lens' influence on system retardance from factors including fabrication stresses, thin film coating contributions, and impacts for opto-mechanical stress. Additionally, objective performance is accurately predicted from individual lens element measurements and data are used to deterministically optimize the system performance.

#### ACKNOWLEDGEMENTS

The authors would like to thank the following people for their efforts related to this work: Keith Hanford, Hieu Ta, and Mike Dunn for their efforts supporting the much of the data collection and analysis in this paper and Bill Furnas, Doug Allan, Bill Rosch, and John Bruning for their teaching and expertise in the fields of polarimetry and birefringent crystals.

#### REFERENCES

- [1] Fahr, S., Werschnik, J., Bening, M., Baldsiefen, T., "Prediction and validation of the polarization performance of high-numerical aperture inspection lenses," Proc. SPIE-OSA 10590, (2017).
- [2] Corning Incorporated, "HPFS<sup>®</sup> Data and Properties," <http://www.corning.com/worldwide/en/products/advanced-optics/product-materials/semiconductor-laser-optic-components/high-purity-fused-silica.html> (April 2018).
- [3] Hellma Materials, GmbH, "Calcium Fluoride, VUV/DUV/UV, VIS and IR applications," <http://www.hellma-materials.com/text/986/en/ausblenden/hellma-materials-calcium-fluoride.html> (April 2018).
- [4] Hinds Instruments, Inc., "Birefringence Measurement Systems," <https://www.hindsinstruments.com/products/birefringence-measurement-systems/> (April 2018).
- [5] Ilis GmbH, "StrainMatic<sup>®</sup> Imaging Polarimeters," <http://www.ilis.de/en/strainmatic.html> (April 2018).
- [6] Burnett, J. H., Levine, Z. H., Shirley, E.L., "Intrinsic birefringence in calcium fluoride and barium fluoride," Physical Review B 64(24): 241102 (2001).
- [7] Goldstein, D. H., [Polarized Light - 3<sup>rd</sup> Edition], CRC Press, Boca Raton, (2011).
- [8] Kliger, D. S., Lewis, J. W., Randall, C. E., [Polarized Light in Optics and Spectroscopy], Academic Press, Inc., San Diego, (1990).
- [9] Dewa, P. D., et al., **Method of assembling optical systems and minimizing retardance distortions in optical assemblies**. US Patent Application (US20180217309A1).
- [10] Oakberg, T.C., "Relative variation of stress-optic coefficient with wavelength in fused silica and calcium fluoride," Proc. SPIE 3754, (1999).